

Article

Effects of Welding Time and Electrical Power on Thermal Characteristics of Welding Spatter for Fire Risk Analysis

Yeon Je Shin  and Woo Jun You *

Department of Architecture & Fire Safety, Dongyang University, Yeongju 36040, Korea; jeje5842@naver.com

* Correspondence: wjyou@dyu.ac.kr; Tel.: +82-54-630-1297

Received: 10 November 2020; Accepted: 4 December 2020; Published: 9 December 2020



Abstract: To predict the fire risk of spatter generated during shielded metal arc welding, the thermal characteristics of welding spatter were analyzed according to different welding times and electrical powers supplied to the electrode. An experimental apparatus for controlling the contact angle between the electrode and base metal as well as the feed rate was prepared. Moreover, the correlations among the volume, maximum diameter, scattering velocity, maximum number, and maximum temperature of the welding spatter were derived using welding power from 984–2067 W and welding times of 30 s, 50 s, and 70 s. It was found that the volume, maximum diameter, and maximum number of welding spatters increased proportionally as the welding time and electrical power increased, but the scattering velocity decreased as the particle diameter increased regardless of the welding time and electrical power. When the measured maximum temperature of the welding spatter was compared with an empirical formula, the accuracy of the results was confirmed to be within $\pm 7\%$ of the experimental constant $C = 112.414 \times P_e^{-0.5045}$. Results of this study indicate quantitatively predicting the thermal characteristics of welding spatter is possible for minimizing the risk of fire spread when the electrode type and welding power is known.

Keywords: shielded metal arc welding; welding spatter; electrode; electrical power; welding time

1. Introduction

Fire risks in construction sites may occur when flammable gases, liquids, or substances reach their ignition points owing to the scattered welding spatter [1–6]. Shielded metal arc welding (SMAW), a method of joining metals by generating an arc and heating the weld metal zone by applying electrical power between the base metal and electrode, has been widely used in industrial sites since the method of SMAW is applied to almost all repairing of cast iron in air or steel under water [7–10]. However, it involves the risk of fire spreading to nearby combustibles caused by high temperatures because the scattered welding spatters are larger comparable to those of gas metal arc welding (GMAW), which uses plasma [11,12]. Especially, the fire hazards from the SMAW at building construction sites can occur when welding spatters make contact with the inward of a pipe or other enclosed space filled with flammable vapor or liquid [12–19]. In addition, the polarity of electrode can cause changes in welding spatter diameter and number [7,19–23]. From the viewpoint of fire technology, analyzing the thermal characteristics of welding spatter is one of the widely used methods to predict fire spread, where related research has already been conducted.

Hagiwara et al. [24,25] conducted an experimental study on the particle size distribution of welding spatter according to the electrical power supplied to the electrode. They found that 90% of the particles had diameters of less than 1 mm and analyzed the fire spread phenomenon in combustibles, such as benzene, acetone, and urethane foam. This study, however, appears to have limitations in

quantitatively analyzing the thermal characteristics of welding spatter crucial to fire risks, which are caused by the electrical power and depend on the particle size.

Hagimoto et al. [19] calculated the particle size according to the electrode diameter when the same electrical power was supplied to the electrode and found that approximately 80% of the particles were scattered to a distance of 0.5 m, 15% to 0.5–1.0 m, and 5% to more than 1 m. They reported that fire can spread to combustibles (urethane foam etc.) when large particles of diameters 0.9–3.0 mm are scattered to a distance of more than 3.5 m.

Brandi et al. [26] analyzed the correlation between the material properties of the electrode core and fire risks using standard mineral dressing techniques. They found that the porosity and density of the welding spatter varied according to the electrical power and stressed the importance of the electrode physical properties for satisfying the ignition requirements of combustibles.

Results from previous studies show that the conditions of fire spread to combustibles during welding vary due to the varying thermal characteristics of welding spatter depending on the electrical power [18,26,27]. Therefore, Shin and You [27] calculated the particle size distribution and mean particle size of welding spatter by assuming a steady-state maximum temperature of the welding spatter for igniting combustibles and proposed an equation for predicting the mean particle temperature based on the energy conservation relationship. According to them, predicting the maximum temperature of the welding spatter is possible when the electrical power, total volume, mean size, and scattering velocity of the particles are known. As these parameters (except the electrical power) vary depending on the electrical power, it is necessary to analyze the relationships among the main factors according to the experimental conditions. This is necessary for the quantitative analysis of the risk of fire spread due to scattered particles. Therefore, in this study, we propose a method for predicting fire risks by quantitatively deriving the thermal characteristics of welding spatter according to the welding time and electrical power.

2. Material and Methods

2.1. Theoretical Approach

Figure 1 shows the schematic of the total volume of the welding spatter during welding. The total mass of the welding spatter ($\Delta m_{p,total}$) can be calculated according to Equation (1) after measuring the mass melted on the base metal ($\Delta m_{b,p}$) and is dependent on the welding time (Δt) and electrical power (P_e). The core inside the electrode is made of steel ($\rho_{\text{iron}} = 7860 \text{ kg/m}^3$) and the coating outside the electrode contains sodium silicate ($\rho_{\text{Sodium Silicate}} = 2400 \text{ kg/m}^3$). However, it is possible to calculate the volume of a single particle (ΔV_i) using the relationship $\Delta V_i = \Delta m_i / \rho_i$ only when the mixed ratios of materials are given for each welding spatter.

$$\Delta m_{p,total} = \Delta m_{el} - \Delta m_{b,p} \quad (1)$$

where Δm_{el} , $\Delta m_{b,p}$, and $\Delta m_{p,total}$ are the masses of the electrode and solidified weld metal attached to the base metal and total mass of scattered particles, respectively. In a previous study, the mean particle temperature was predicted by assuming the steady-state condition of the initial temperature of welding spatter as the maximum value for the ignition combustibles, as shown in Equation (2) [27].

$$T_{p,s} = T_{\infty} + \frac{P_e - \sigma \varepsilon A_{b,s} (T_{s,b}^4 - T_{sur}^4)}{NhA_{p,s}} \quad (2)$$

where $T_{p,s}$, T_{∞} , T_{sur} , P_e , σ , ε , $A_{b,s}$, $T_{s,b}$, N , h , and $A_{p,s}$ are the mean particle temperature, surrounding temperature, surface temperature, electrical power (P_e), Stefan–Boltzmann constant, emissivity, surface area and surface temperature of base metal, average number of particles, convective heat

transfer coefficient, and surface area of particle, respectively. The mean particle size, $d_{p,m}$, and convective heat transfer coefficient, h , can be obtained using Equations (3) and (4), respectively [14,27,28].

$$N = \frac{6V_{p,total}}{\pi d_{p,m}^3} \quad (3)$$

$$Nu_D = \frac{hd_{p,m}}{k} = 2 + 0.6Re_D^{0.5}Pr^{1/3} \quad (4)$$

where $V_{p,total}$, $d_{p,m}$, Nu_D , k , Re , and Pr are the total volume of particles, mean diameter of particles, Nusselt number, thermal conductivity, Reynolds number ($Re_D = \rho u_{p,m} d_{p,m} / \mu$), and Prandtl number ($Pr = C_p \mu / k$), respectively. Therefore, the temperature distribution prediction shown in Equation (2) is possible when $V_{p,total}$, $d_{p,m}$, and $u_{p,m}$ can be calculated using Equations (3) and (4). As the total volume, mean diameter, and scattering velocity of particles vary according to the welding time and electrical power, the functional relationship given by Equation (5) must be also determined [14,27].

$$N, d_m, h \sim f(P_e, \Delta t) \quad (5)$$

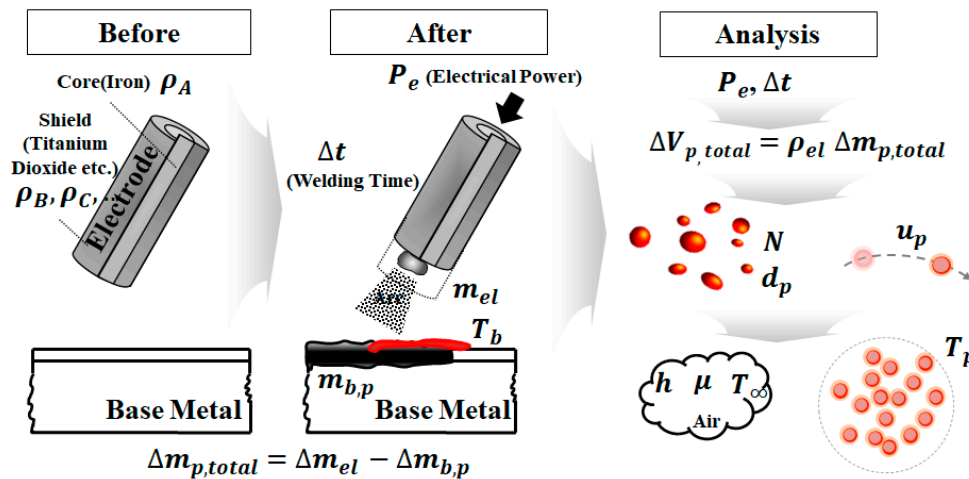


Figure 1. Schematic of welding spatter in shielded metal arc welding (SMAW) and assumptions for energy balance between particles and base metal.

2.2. Experimental Apparatus

Figure 2 shows the semi-automated SMAW experimental apparatus, which was constructed by maintaining perpendicularity between the electrode and base metal constant (welding angle $\theta = 90^\circ$) and specifying the maximum feed rate of the welding torch as 7 mm/s. This made it possible to analyze the size and scattering velocity of the particles. As shown in the figure, welding spatters were scattered under different welding times (Δt) and electrical power (P_e), and the scattering velocity and mean temperature of the welding spatters were measured using a high-speed camera (model: phantom Miro M/R/LC310, USA) and a thermal imaging camera (model: Fluke Tix501). The scattering velocity and mean temperature of the welding spatter were measured using a high-speed camera (model: phantom LC310) and a thermal imaging camera (model: Fluke Tix501). The particle size distribution was determined using Image J software after collecting all welding spatter in a $50 \times 46 \times 64 \text{ cm}^3$ acrylic box. Table 1 lists the specifications of the experimental apparatus and the experimental conditions for the average values of three times results are denoted in Table 2.

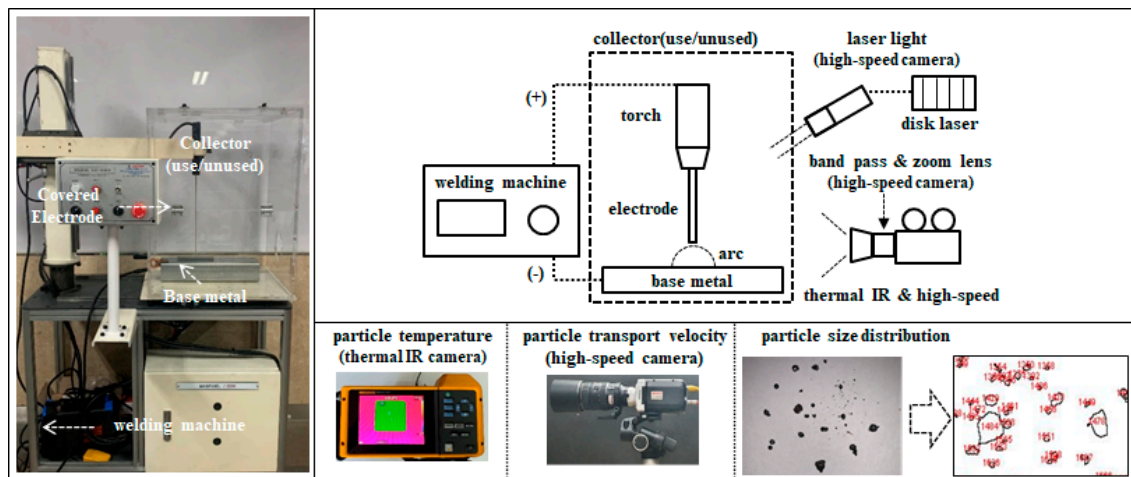


Figure 2. Schematic and images of experimental apparatus for welding spatter analysis.

Table 1. Specifications of experiment apparatus.

Equipment	Specification
Welding machine	Output current (20~220) A, Rated input voltage 220 V, Electric power (0~2.5) kW Rated duty cycle 60%, Model: Rolwal MMA-200E
Thermal imaging camera	Infrared resolution 640 × 480, Temp. measurement range −20 to 650 °C, Accuracy ±2 °C or 2%, Frame rate 60 Hz, Model: Fluke Tix 501
High-speed camera	Resolution 640 × 480, Sampling rate 10,000 fps, Model: phantom Miro M/R/LC310 Lens: Nikon 105 mm, 2× converter
Electronic energy meter	Band-pass filter: Φ 50 mm, 810 nm/12 nm, CN code 90022000
Precision balance	230 AC, 60 Hz, 16 A/3680 W (Model: KEM2500) Max. load weight 320 g, Accuracy 0.1 mg, Model: PX224KR
Electrode	High titanium oxide type electrode (AWS E-6013) Core: Iron (65–75%), Coating: Titanium dioxide (10–15%), Feldspar (5–10%), Mn (1–5%), Sodium silicate (1–5%), Limestone (1–5%), Mica (1–5%)

Table 2. Experimental conditions to study the effects of thermal characteristics of welding spatter on the welding time and electrical power.

Test Number	Welding Time, Δt (s)	Welding Current (A)	Welding Voltage (V)	Electrical Power, P_e (W)
Case #1	30	80	12	984
Case #2	50			
Case #3	70			
Case #4	30	100	13	1337.3
Case #5	50			
Case #6	70			
Case #7	30	130	14	1802.0
Case #8	50			
Case #9	70			
Case #10	30	150	17	2067.5
Case #11	50			
Case #12	70			

Welding polarity: DC-, Contact angle: 90°, Arc length: 5 mm, Base metal: Mild steel (SS400); Electrode diameter, d_{el} : 4.0 mm, Material properties of electrode given in Table 1.

3. Results and Discussion

3.1. Volume of Welding Spatter

Figure 3 shows the variation of the measured reduction rate (u_{rate}) of the electrode length according to the electrical power (P_e) in the case of welding times (Δt) of 30 s, 50 s, and 70 s. It is seen that as P_e increased, u_{rate} also increased proportionally as the mass of the electrode welded to the base metal ($\Delta m_{b,p}$) increased. When P_e was constant, a constant value of u_{rate} was calculated, which was consistent with that obtained using Equation (6) within $\pm 4\%$ for the average values u_{rate} regardless of Δt .

$$u_{rate} = a_1 + b_1 \times P_e \quad (6)$$

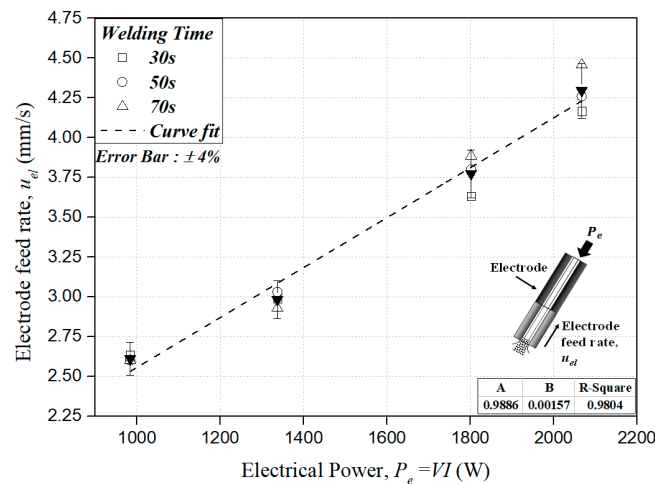


Figure 3. Electrode feed rate depending on the electrical power for welding time = 30 s, 50 s, and 70 s.

Here, a_1 and b_1 are experimental constants. It is estimated that $a_1 = 0.989$ mm/s and $b_1 = 0.157 \times 10^{-2}$ W-mm/s are obtained according to the base metal and electrode specifications listed in Table 1, and the electrical power ranges between 984 and 2067 W.

Figure 4 shows the variation in the measured mass loss of the electrode (Δm_{el}) and the mass welded to the base metal ($\Delta m_{b,p}$) according to the electrical power (P_e) for the welding times (Δt) of 30 s, 50 s, and 70 s. In this figure, the symbols enclosed in brackets represent Δm_{el} , which increased proportionally to u_{rate} . When Δt increased keeping P_e constant, Δm_{el} increased in proportion to u_{rate} . Therefore, when Equation (6) and the electrode density measured using a load cell ($\rho = 4726$ kg/m³) are applied, Δm_{el} is given by Equation (7) expressed by the dotted line, which agrees with the measured value within an error range of approximately $\pm 5\%$.

$$\Delta m_{el} = u_{rate} \times \Delta t \times \left(\frac{\pi}{4} d_{el}^2 \right) \times \rho_{el} \quad (7)$$

where d_{el} is the electrode diameter is used as the reference value of 4.0 mm. Notably in the figure, the measured value of $\Delta m_{b,p}$ increased in proportion to the magnitudes of Δt and P_e , as shown by the closed symbol value. In addition, 88.6% Δm_{el} was found to be welded to the base metal on average. This result indicates that approximately 11.4% Δm_{el} was responsible for generating welding spatter when P_e was supplied to the electrode. The energy transmitted to the electrode can be simplified through the assumption shown in Equation (8).

$$\sigma \varepsilon A_{b,s} (T_{s,b}^4 - T_{sur}^4) \equiv 0.886 P_e \quad (8)$$

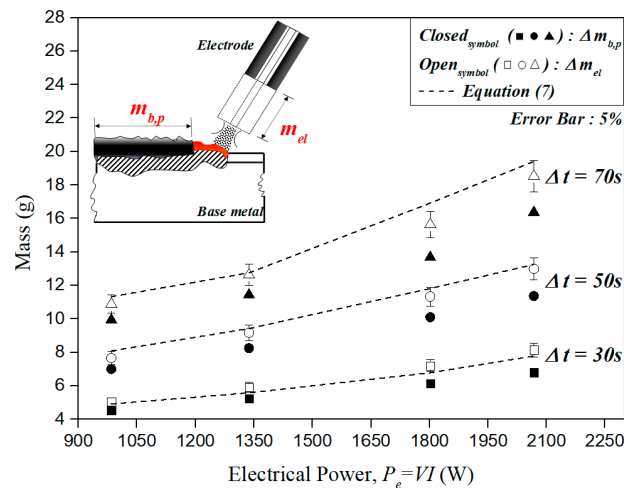
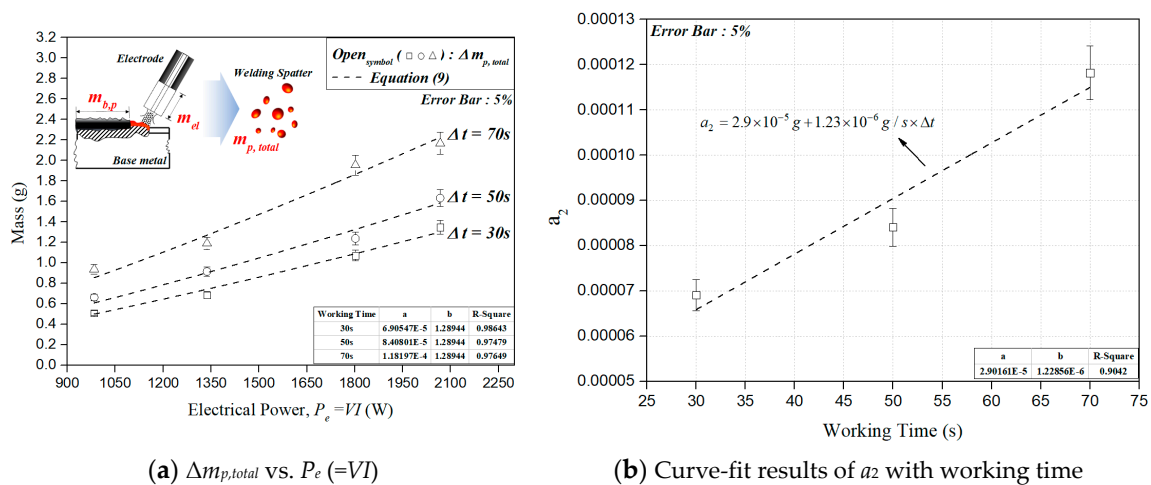


Figure 4. Experimental variation of Δm_{el} and $\Delta m_{b,p}$ according to P_e for $\Delta t = 30$ s, 50 s, and 70 s.

Figure 5a shows the variation of the total mass of the particles scattered from the electrode ($\Delta m_{p,total}$) using Equation (1), mass reduction of the electrode (Δm_{el}), and mass welded to the base metal ($\Delta m_{b,p}$) for the welding times (Δt) of 30 s, 50 s, and 70 s according to the electrical power. The result of curve-fitting the calculated values of $\Delta m_{p,total}$ with increasing electrical power (P_e) under the same Δt values is shown in Equation (9).

$$m_{p,total} = a_2 \cdot P_e^{b_2} \tag{9}$$



(a) $\Delta m_{p,total}$ vs. $P_e (=VI)$

(b) Curve-fit results of a_2 with working time

Figure 5. Effects of electrical power on the total mass of welding particles at welding times of 30 s, 50 s, and 70 s.

It was found that a_2 is related to Δt as shown in Figure 5b, and this tendency is shown in Equation (10) when b_2 is constant at 1.28944.

$$a_2 = 2.9 \times 10^{-5} \text{g} + 1.23 \times 10^{-6} \text{g/s} \times \Delta t \tag{10}$$

Figure 6 shows the density values (ρ_i) of a single scattered welding particle measured by calculating the mass ($m_{p,i}$) and volume ($\Delta V_{p,i}$) of the particle using diameters ($d_{p,i}$) of 1.736, 2.023, 2.294, and 2.352 mm. Because the electrode contains various metal components, as shown in Table 1, ρ_i may vary depending on the material composition inside the shield and core [26,29]. In particular, the mass proportions of metals that constitute each particle must be determined to obtain the total volume of scattered welding spatter ($\Delta V_{p,total}$), but limitations exist in analyzing the density when

measuring each mixed component for at least 1000 small particles with a diameter of 0.1 mm or less. Therefore, we attempted to analyze the thermal characteristics of welding spatter by assuming $\rho_{p,total} \equiv \rho_{el}$ (4726 kg/m³) and calculating $\Delta V_{p,total}$ as shown in Equation (11).

$$\Delta V_{p,total} = \frac{\Delta m_{p,total}}{\rho_{el}} = \frac{(2.9 \times 10^{-5} + 1.23 \times 10^{-6} \times \Delta t) \times P_e^{b2}}{\rho_{el}} \tag{11}$$

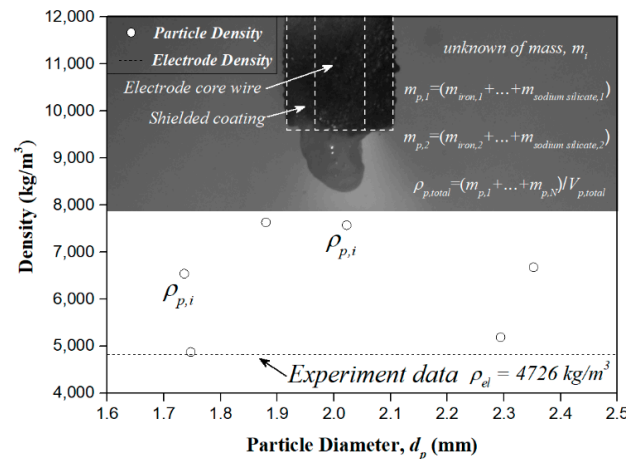
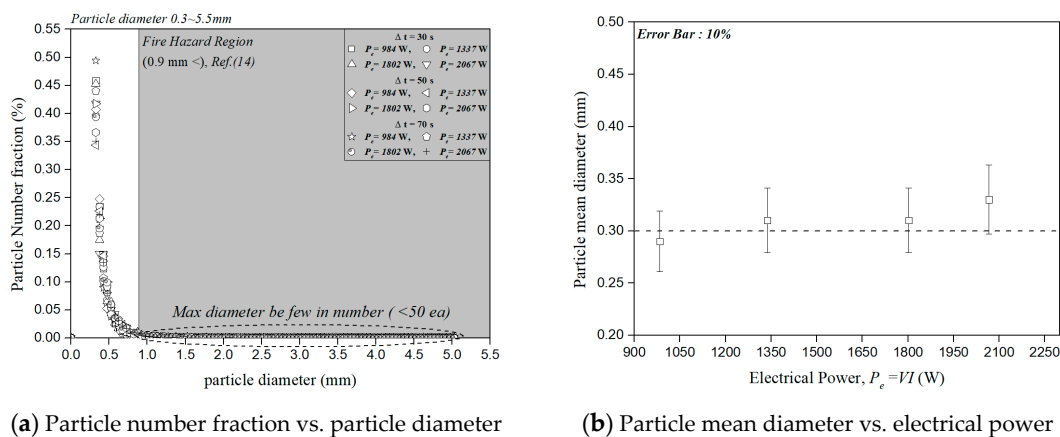


Figure 6. Measured value of one particle density using $d_p = 1.73\text{--}2.35$ mm.

3.2. Diameter and Number of Welding Spatters

Figure 7 shows the fraction (N_i/N_{total}) of the number of particles, which is the ratio of particles with diameter (N_i) to the total number of scattered particles (N_{total}), according to P_e at $\Delta t = 30$ s, 50 s, and 70 s. As mentioned before, the particle size distribution was determined using Image J software after collecting welding spatter in a $50 \times 46 \times 64$ cm³ acrylic space, and it was analyzed by excluding the diameters of 0.3 mm or less due to the resolution. It was found that the mean particle diameter ($d_{p,m}$) was approximately 0.3 mm regardless of Δt and P_e , which is similar to the results of previous studies ($d_{p,m} < 0.5$ mm) [9,11]. Therefore, the mean number of particles (N) can be calculated using Equation (4). The main purpose of this study was to predict fire risks according to the thermal characteristics of scattered particles; however, the mean number of particles (N) was expressed using the maximum number of particles (N_{max}) to analyze the thermal characteristics according to the maximum particle diameter ($d_{p,max}$) generated during welding.



(a) Particle number fraction vs. particle diameter

(b) Particle mean diameter vs. electrical power

Figure 7. Results of the (a) fraction of particle number, and (b) particle mean diameter when $P_e = 984, 1337, 1802,$ and 2067 W and $\Delta t = 30$ s, 50 s, and 70 s.

As the maximum particle size, $d_{p,max}$, is still undetermined, it is necessary to analyze $d_{p,max}$ according to Δt and P_e to solve Equation (12).

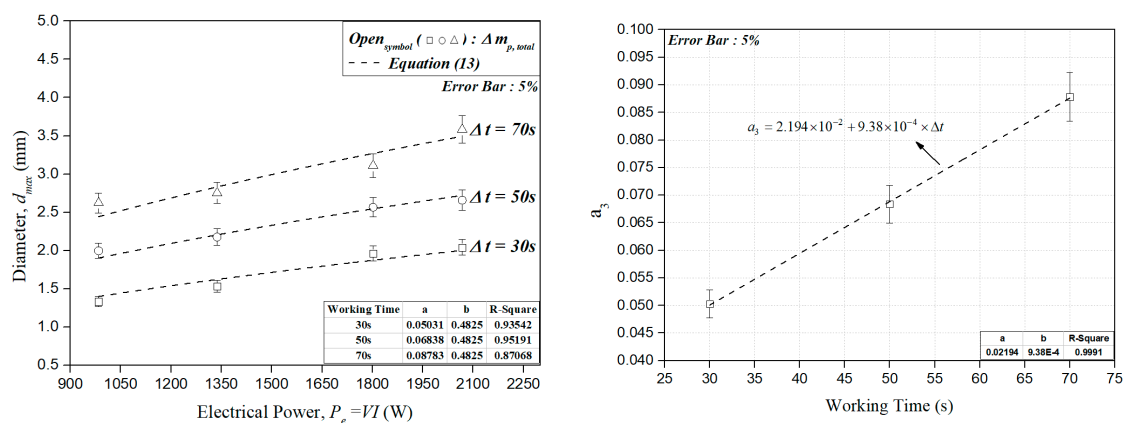
$$N_{max} = \frac{6V_{total}}{\pi d_{p,max}^3}, N = N_{max} (d_{p,max} / d_{p,m})^3 \tag{12}$$

Figure 8 shows the results of analyzing the maximum diameter of scattered particles ($d_{p,max}$) according to the electrical power (P_e) at $\Delta t = 30$ s, 50 s, and 70 s. Each measured value represents the average of the maximum diameter obtained in three repeated experiments. Apparently, the size of the particles scattered from the electrode increased as Δt increased under a constant P_e because the temperature around the weld zone of the base metal increased. In addition, under the same Δt , the size of scattered particles increased in proportion to the melted mass of the electrode as P_e increased as shown in Equation (13).

$$d_{p,max} = a_3 \times P_e^{b_3} \tag{13}$$

where a_3 and b_3 are experimental constants. When $b_3 = 0.4825$, a_3 can be calculated by Equation (14) and plotted in Figure 8b.

$$a_3 = 2.194 \times 10^{-2} + 9.38 \times 10^{-4} \times \Delta t \tag{14}$$



(a) Maximum particle diameter vs. electrical power

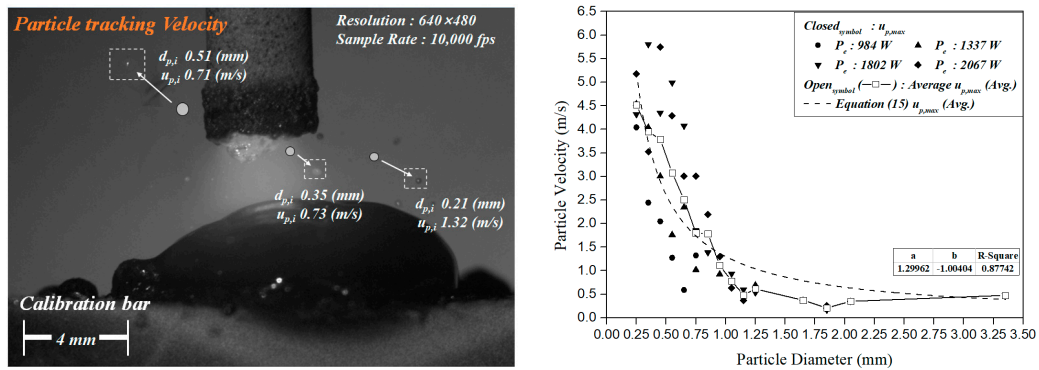
(b) The experiment coefficient of a_3 vs. Welding time

Figure 8. Effects of electrical power on the distribution of the particles and the max diameter of the particles at welding time = 30 s, 50 s, and 70 s.

3.3. Velocity of Welding Spatter

Figure 9a shows the results of measuring the mean particle velocity according to the particle diameter under an electrical power of 984 W using a high-speed camera (model: phantom LC310) and particle tracking velocimetry (PTV). It is observed that the scattering velocity showed a tendency to decrease as the particle diameter increased under the experimental conditions of the welding time (Δt) and electrical power (P_e), as shown in Table 2. The correlation between the maximum diameter of scattered particles ($d_{p,max}$) and the scattering velocity ($u_{p,max}$) was analyzed, as shown in Figure 9b. $u_{p,max}$ decreased as $d_{p,max}$ increased with a difference of less than $\pm 10\%$ depending on the values of Δt and P_e , and the relationship shown in Equation (15) was found.

$$u_{p,max} = 1.3 \times d_{p,max}^{-1.004} \tag{15}$$



(a) Velocity contour of welding particle (b) Particle velocity vs. particle diameter

Figure 9. Results of the particle velocity according to the particle diameter.

3.4. Thermal Characteristics of Welding Spatter

Using the results of the total volume of particles ($V_{p,total}$), maximum number of particles (N_{max}), particle diameter ($d_{p,max}$), and scattering velocity ($u_{p,max}$) according to the Δt and P_e obtained in Section 3.1 to determine the convective heat transfer coefficient shown in Equation (4), Equation (16) can be formed.

$$h_{max} = (2 + 0.6Re_{d,max}^{0.5}Pr^{1/3})k(T_{ref})/d_{p,max}, \quad (16)$$

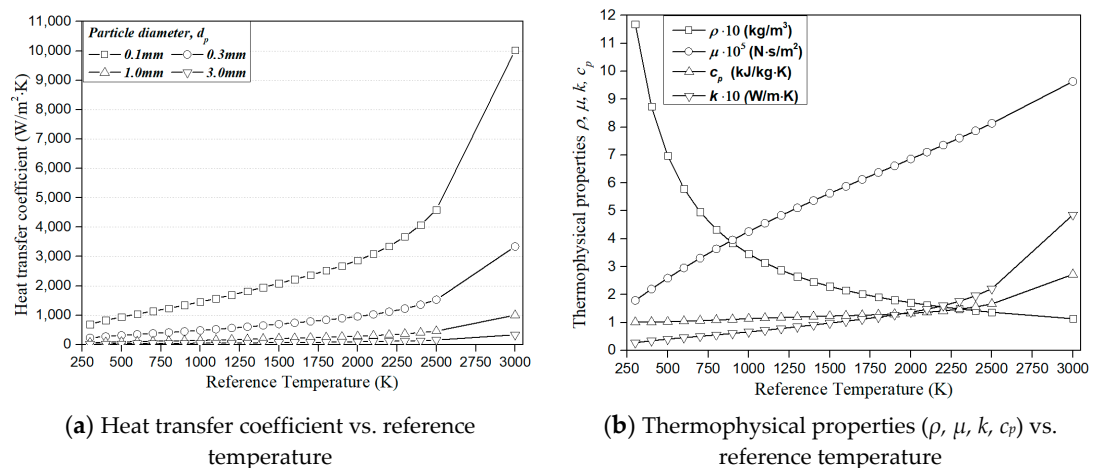
where $Re_{d,max}$ is the Reynolds number ($Re_{d,max} = \rho_p u_{p,max} d_{p,max} / \mu$) considering the maximum particle diameter ($d_{p,max}$). In particular, the thermal conductivity (k), specific heat (C_p), viscosity (μ), and density (ρ) of air vary depending on the reference temperature ($T_{ref} = (T_{p,s} + T_{\infty})/2$), as shown in Figure 10a. In this study, these can be calculated using Equations (17)–(20) based on the data given by this study [30].

$$k(T_{rep}) = -7.16 \times 10^{-3} + 1.72 \times 10^{-4} \times T - 2.45 \times 10^{-7} \times T^2 + 2.29 \times 10^{-10} \times T^3 - 9.81 \times 10^{-14} \times T^4 + 1.63 \times 10^{-17} \times T^5 \quad (17)$$

$$c_p(T_{rep}) = 1.05 - 2.89 \times 10^{-4} \times T + 6.83 \times 10^{-7} \times T^2 - 3.4 \times 10^{-10} \times T^3 + 2.25 \times 10^{-14} \times T^4 + 1.55 \times 10^{-17} \times T^5 \quad (18)$$

$$\mu(T_{rep}) = 4.26 \times 10^{-6} + 4.93 \times 10^{-8} \times T - 1.33 \times 10^{-11} \times T^2 + 2.36 \times 10^{-15} \times T^3 \quad (19)$$

$$\rho(T_{rep}) = 374.074 \times T^{-1.0114} \quad (20)$$



(a) Heat transfer coefficient vs. reference temperature (b) Thermophysical properties (ρ, μ, k, c_p) vs. reference temperature

Figure 10. Effects of the heat transfer coefficient of the maximum particle diameter and velocity according to thermophysical properties (ρ, μ, k, c_p).

Figure 10a shows the results of analyzing the convective heat transfer coefficient, h , according to T_{ref} when $d_{p,max} = 0.1, 0.3, 1.0,$ and 3.0 mm. h decreased as $d_{p,max}$ increased while the scattering velocity ($u_{p,max}$) decreased to 13.12, 4.35, 1.30, and 0.43 m/s at different $d_{p,max}$ values obtained by Equation (15). Therefore, Equation (2), for calculating the mean particle temperature considering the welding time and electrical power, can be expressed as in Equation (21).

$$T_{p,s} = T_{\infty} + \frac{0.13P_e}{N_{max}h_{max}A_{p,max}r_{ratio}}, \tag{21}$$

where $N_{max}, h_{max}, A_{p,max},$ and r_{ratio} are the total number of particles, heat transfer coefficient, surface area of a particle, and a constant calculated by replacing $d_{p,m}$ with $d_{p,max}$, respectively, when welding particles are at their maximum size. In particular, the mean number of particles (N) used in Equation (3) and the mean surface area ($A_{p,m}$) are related as $N = N_{max}(d_{-p,m}/d_{-p,max})^{-3}$ and $A_{p,m} = A_{p,max}(d_{-p,m}/d_{-p,max})^2$, whereas the convective heat transfer coefficient (h) for determining the temperature of the welding spatter is given by $h = h_{max} \times (d_{-p,m}/d_{-p,max})^{-0.5} \times (u_{p,m}/u_{p,max})^{0.5}$. Therefore, r_{ratio} is related as,

$$r_{ratio} \sim \left(\frac{u_{p,m}}{u_{p,max}}\right)^{0.5} \left(\frac{d_{p,m}}{d_{p,max}}\right)^{-1.5}, \tag{22}$$

where, $u_{p,m}/u_{p,max}$ represents the ratio of the mean velocity to the maximum velocity. As it varies depending on the diameter, it can be expressed as Equation (23).

$$\left(\frac{u_{p,m}}{u_{p,max}}\right)^{0.5} = C \left(\frac{d_{p,m}}{d_{p,max}}\right)^{0.5}, \tag{23}$$

where C is the experimental constant which may vary depending on the velocity difference. Because $k, C_p, \mu,$ and ρ used to obtain the convective heat transfer coefficient are functions of $T_{p,s}$ as shown in Equations (17)–(20), it is necessary to solve Equation (13) for the maximum particle size, Equation (15) for the maximum velocity, Equation (16) for the convective heat transfer coefficient, and Equation (23) to perform iterative calculations for predicting the maximum temperature of the welding spatter.

Figure 11a shows the results of maximum temperature ($T_{p,max}$) measured by capturing the welding spatter images accumulated on the acrylic collection plate at 60 fps for 70 s using a thermal imaging camera (Model: Fluck Ti520) at $\Delta t = 70$ s and $P_e = 1337$ W. As shown in the figure, the approximate maximum and mean particles were 432 °C and 347 °C, respectively.

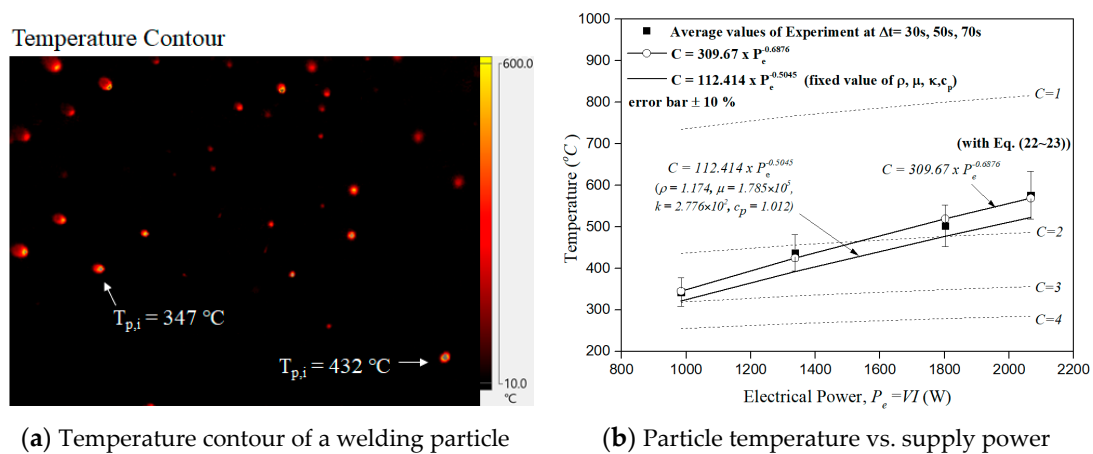


Figure 11. The results of temperature contour and the comparison of the prediction with experiment values of C .

Figure 11b shows the results calculated using the maximum particle temperature measurements and Equation (21) under the experimental conditions of Δt and P_e shown in Table 2. The experimental values agreed with the mean values with a difference of up to $\pm 10\%$ depending on Δt , and the temperature tended to increase as P_e increased. It should be noted that the maximum difference due to the time change was small (within $\pm 2\text{C}$) as shown in Equation (21) when C was constant, but the increasing tendency of the temperature in proportion to P_e was found to be consistent with the experimental values. However, when the values of C were 1, 2, 3, and 4, the slope at which the maximum particle temperature increased over the increase in P_e was smaller than the experimental value. This appears to be due to different values of C when the difference between the mean and maximum scattering velocities of the welding spatter increased along with P_e . At each P_e , the value of C can be obtained using Equations (24) and (25).

$$C_1 = 309.67 \times P_e^{-0.6876} \quad (24)$$

$$C_2 = 112.414 \times P_e^{-0.5045} \quad (25)$$

C_1 is a constant calculated by performing iterative calculations using Equations (17)–(20) for predicting the maximum particle temperature, whereas C_2 is calculated using the values of the density, thermal conductivity, viscosity coefficient, and specific heat at room temperature (298 K). Therefore, the maximum particle temperature can be predicted within an error range of approximately 5% using the equation to solve C_2 .

Figure 12 shows the results of calculating the maximum temperature and diameter of the welding particles when the welding time (Δt) ranged from 30–70 s and P_e from 984–2067.5 W. “Fire hazard region” means the possibility of fire spreading to combustible materials such as polyurethan foam as mentioned in Ref [14,15,27], and “No ignition region” means the minimized conditions of fire spread. Based on previous studies, it can be confirmed that the maximum welding time and electrical power are 10 s and 1150 W, respectively, when the minimum particle size of welding spatter for the risk of fire spread is 0.9 mm, and the minimum temperature is 350 °C [19]. Therefore, the results of this study indicate that it is possible to calculate the electrical power for minimizing the risk of fire due to welding spatter when the electrode type and welding time are known.

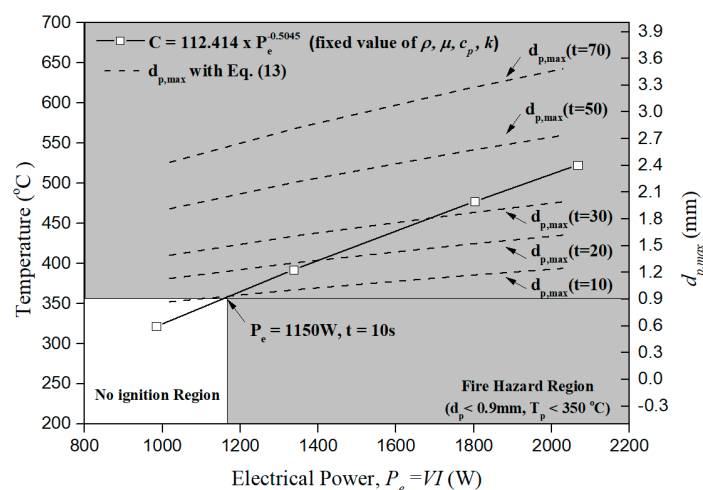


Figure 12. Predicted results of the maximum diameter and temperature of the welding particle depending on the electrical power and welding time.

4. Summary

In this study, the volume, maximum diameter, scattering velocity, and maximum number of welding spatter for shielded metal arc welding (SMAW) were analyzed according to the electrical

power and welding time. When the electrical power was varied for welding times of 30 s, 50 s, and 70 s, the following results were derived.

First, when the mass of the electrode and scattered particles was calculated, an empirical formula was derived, which showed an increase in the mass of scattered particles when the electrical power increased at a constant welding time. In particular, the mass of scattered welding spatter represented approximately 11.45% of the total mass of the consumed electrode on average. The densities of the scattered particles were found to vary between 4876–7572 kg/m³ depending on the volume fraction of the core and coating composition of the electrode as referred by manufacturer.

Second, it was found that the mean diameter of welding spatter was approximately 0.3 mm, which was constant regardless of the welding time and electrical power. The maximum particle size, which has an important impact on fire risks, however, showed a tendency to increase in proportion to the welding time and electrical power. An empirical formula considering the maximum particle size was also derived to predict the temperature of the scattered welding spatter.

Third, the scattering velocity differed with differences of up to ±91% according to the welding time and electrical power. This appears to be due to the fact that materials with significantly different densities were mixed, which affected the momentum of the welding spatter while they were generated from the electrode. However, the scattering velocity decreased as the particle diameter increased.

Fourth, empirical formulas for the volume, maximum diameter, and scattering velocity of the welding spatter according to the welding time and electrical power were derived and compared with the maximum temperature measurements during the welding process. Results showed a good agreement between the compared values within an error range of approximately 10%. After verifying this accuracy, the case in which the minimum temperature of welding spatter was 350 °C or higher and the particle size was 0.9 mm was analyzed. It was found that fire risks can be minimized when a maximum welding time of 10 s and maximum electrical power of 1150 W are used. It should be noted that the maximum temperature of the welding spatter increased in proportion to the electrical power regardless of the welding time. The results of this study are expected to be used as important data for quantitatively presenting measures to minimize the fire risk of welding spatter.

Author Contributions: Conceptualization, Y.J.S. and W.J.Y.; Data curation, W.J.Y.; Formal analysis, W.J.Y.; Funding acquisition, W.J.Y.; Investigation, Y.J.S.; Methodology, W.J.Y.; Project administration, W.J.Y.; Software, Y.J.S.; Supervision, W.J.Y.; Validation, Y.J.S. and W.J.Y.; Visualization, Y.J.S.; Writing—original draft, Y.J.S.; Writing—review & editing, W.J.Y. All authors have read and agreed to the published version of the manuscript.

Funding: This research was funded by Korea Agency for Infrastructure Technology Advancement, grant number (19CTAP-C151893-01).

Conflicts of Interest: The authors declare no conflict of interest. The funders had no role in the design of the study; in the collection, analyses, or interpretation of data; in the writing of the manuscript, or in the decision to publish the results.

References

1. Messler, R.W., Jr. *Principles of Welding: Processes, Physics, Chemistry, and Metallurgy*; Wiley: London, UK, 2008.
2. DuPont, J.N.; Lippold, J.C.; Kiser, S.D. *Welding Metallurgy and Weldability of Nickel-Base Alloys*; Wiley: London, UK, 2009.
3. Weman, K. *Welding Processes Handbook*, 2nd ed.; Cambridge Woodhead Publishing: Cambridge, UK, 2003.
4. Babrauskas, V. *Ignition Handbook: Principles and Applications to Fire Safety Engineering, Fire Investigation, Risk Management, and Forensic Science*; Fire Science Publishers: Issaquah, WA, USA, 2003.
5. National Fire Protection Association (NFPA). *NFPA Standard 51B: Standard for Fire Prevention During Welding, Cutting, and Other Hot Work, Technical Report*; National Fire Protection Association: Quincy, MA, USA, 2009.
6. Schonherr, W. Fire risks with welding torches and manual arc welding-globules, spatter and how far they can be thrown. *Schweiss. Schneid.* **1982**, *34*, E74–E77.
7. Tomków, J.; Fydrych, D.; Wilk, K. Effect of Electrode Waterproof Coating on Quality of Underwater Wet Welded Joints. *Materials* **2020**, *13*, 2947. [[CrossRef](#)] [[PubMed](#)]

8. Srisuwan, N.; Kumsri, N.; Yingsamphancharoen, T.; Kaewvilai, A. Hardfacing welded ASTM A572-based, high-strength low-alloy steel: Welding, characterization, and surface properties related to the wear resistance. *Metals* **2019**, *9*, 244. [[CrossRef](#)]
9. Omajene, J.E.; Martikainen, J.; Kah, P.; Pirinen, M. Fundamental difficulties associated with underwater wet welding. *Int. J. Eng. Res. Appl.* **2014**, *4*, 26–31.
10. Łabanowski, J.; Fydrych, D.; Rogalski, G.; Samson, K. Underwater welding of duplex stainless steel. *Solid State Phenom.* **2012**, *183*, 101–106. [[CrossRef](#)]
11. Janusas, G.; Jutas, A.; Palevicius, A.; Zizys, D.; Barila, A. Static and vibrational analysis of the GMAW and SMAW joints quality. *J. Vibroeng.* **2012**, *14*, 1220–1226.
12. Urban, J.L. Spot Ignition of Natural Fuels by Hot Metal Particles. Ph.D. Theses, University of California Berkeley, Berkeley, CA, USA, 2017.
13. Mikkelsen, K. An Experimental Investigation of Ignition Propensity of Hot Work Processes in the Nuclear Industry. Master's Thesis, University of Waterloo, Waterloo, ON, Canada, 2014.
14. Song, J.; Wang, S.; Chen, H. Safety distance for preventing hot particle ignition of building insulation materials. *Theor. Appl. Mech. Lett.* **2014**, *4*, 034005. [[CrossRef](#)]
15. Urban, J.L. Spot Fire Ignition of Natural Fuels by Hot Aluminum Particles. *Fire Technol.* **2017**, *54*, 797–808. [[CrossRef](#)]
16. Liu, Y.; Urban, J.L.; Xu, C.; Fernandez-Pello, C. Temperature and Motion Tracking of Metal Spark Sprays. *Fire Technol.* **2019**, *55*, 2143–2169. [[CrossRef](#)]
17. Kim, Y.S.; Eagar, T.W. Analysis of metal transfer in gas metal arc welding. *Weld. J.* **1993**, *72*, 269-s.
18. Tanaka, T. On the inflammability of combustible materials by welding spatter. *Rep. Natl. Res. Inst. Police Sci.* **1977**, *30*, 51–58.
19. Hagimoto, N.; Kinoshita, K. Scattering and Igniting Properties of Sparks Generated in an Arc Welding. In *6th Indo Pacific Congress on Legal Medicine and Forensic Sciences*; Indo Pacific Association of Law, Medicine and Science: Kobe, Japan, 1998; pp. 863–866.
20. Shigeta, M.; Peansukmanee, S.; Kunawong, N. Qualitative and quantitative analyses of arc characteristics in SMAW. *Weld. World* **2016**, *60*, 355–361. [[CrossRef](#)]
21. Pistorius, P.G.; Liu, S. Changes in Metal Transfer Behavior during Shielded Metal Arc Welding. *Weld. J.* **1997**, *76*, 305–315.
22. Narasimhan, P.N.; Mehrotra, S.; Raja, A.R.; Vashista, M.; Yusufzai, M.Z.K. Development of hybrid welding processes incorporating GMAW and SMAW. *Mater. Today Proc.* **2019**, *18*, 2924–2932. [[CrossRef](#)]
23. Xu, X.; Liu, S.; Bang, K.S. Comparison of metal transfer behavior in electrodes for shielded metal arc welding. *Int. J. Korean Weld. Soc.* **2004**, *4*, 15–22.
24. Hagiwara, T.; Yamano, K.; Nishida, Y. Ignition risk to combustibles by welding spatter. *J. Jpn. Assn. Fire Sci. Eng.* **1982**, *32*, 8–12.
25. Kinoshita, K.; Hagimoto, Y. Temperature measurement of falling spatters of arc welding. In *Proceedings of the 22nd Annual Meeting Japan Society for Safety Engineering*, Japan Society for Safety Engineering, Tokyo, Japan; 1989; pp. 145–148.
26. Brandi, B.; Taniguchi, C.; Liu, S. Analysis of metal transfer in shielded metal arc welding. *Suppl. Weld. J.* **1991**, *70*, 261s–270s.
27. Shin, Y.J.; You, W.J. Analysis of the thermal characteristics of welding spatters in SMAW using simplified model in fire technology. *Energies* **2020**, *13*, 2266. [[CrossRef](#)]
28. Ranz, W.E.; Marshall, W.R. Evaporation from drop, Part 1. *Chem. Eng. Prog.* **1952**, *48*, 141–146.
29. Marques, E.S.V.; Silva, F.J.G.; Paiva, O.C.; Pereira, A.B. Improving the mechanical strength of ductile cast iron welded joints using different heat treatments. *Materials* **2019**, *226*, 2263. [[CrossRef](#)] [[PubMed](#)]
30. Incropera, F.P.; Lavine, A.S.; Bergman, T.L.; DeWitt, D.P. *Principles of Heat and Mass Transfer*; Wiley: Hoboken, NJ, USA, 2013.

Publisher's Note: MDPI stays neutral with regard to jurisdictional claims in published maps and institutional affiliations.



© 2020 by the authors. Licensee MDPI, Basel, Switzerland. This article is an open access article distributed under the terms and conditions of the Creative Commons Attribution (CC BY) license (<http://creativecommons.org/licenses/by/4.0/>).